International Journal of Greenhouse Gas Control 7 (2012) 89–97

Contents lists available at SciVerse ScienceDirect

International Journal of Greenhouse Gas Control

journal homepage: www.elsevier.com/locate/ijggc

Sequestration of non-pure carbon dioxide streams in iron oxyhydroxide-containing saline repositories

S. Garcia[a,*], R.J. Rosenbauer[b], J. Palandri[c], M.M. Maroto-Valer[a]

[a] Centre for Innovation in Carbon Capture and Storage (CICCS), Energy and Sustainability Research Division, Faculty of Engineering, University of Nottingham, University Park, Nottingham NG7 2RD, United Kingdom
[b] US Geological Survey, 345 Middlefield Road, Menlo Park, CA 94025, USA
[c] Department of Geological Sciences, 1272 University of Oregon, Eugene, OR 97403, USA

ARTICLE INFO

Article history:
Received 31 January 2011
Received in revised form
27 November 2011
Accepted 2 December 2011

Keywords:
CO_2 storage
Mineral trapping
Saline aquifers
SO_2

ABSTRACT

Iron oxyhydroxide, goethite (α-FeOOH), was evaluated as a potential formation mineral reactant for trapping CO_2 in a mineral phase such as siderite ($FeCO_3$), when a mixture of CO_2–SO_2 flue gas is injected into a saline aquifer. Two thermodynamic simulations were conducted, equilibrating a CO_2–SO_2 fluid mixture with a NaCl-brine and Fe-rich rocks at 150 °C and 300 bar. The modeling studies evaluated mineral and fluid composition at equilibrium and the influence of pH buffering in the system. Results show siderite precipitates both in the buffered and unbuffered system; however, the presence of an alkaline pH buffer enhances the stability of the carbonate. Based on the model, an experiment was designed to compare with thermodynamic predictions. A CO_2–SO_2 gas mixture was reacted in 150 ml of NaCl–NaOH brine containing 10 g of goethite at 150 °C and 300 bar for 24 days. Mineralogical and brine chemistry confirmed siderite as the predominant reaction product in the system. Seventy-six mg of CO_2 are sequestered in siderite per 10 g of goethite.

1. Introduction

Carbon capture and storage (CCS) has the potential to reduce anthropogenic CO_2 emissions to the atmosphere as one strategy in a larger portfolio of options to maintain the use of fossil fuels as an energy source in the short-term while future non-fossil based energy systems are developed and implemented (IPCC, 2005; Lackner et al., 1998; Maroto-Valer, 2010a,b; Mazzotti et al., 2009). Storage of CO_2 in deep-saline aquifers has great potential because of their worldwide occurrence in sedimentary basins and large storage capacity compared to hydrocarbon reservoirs (Bachu and Adams, 2003; Bradshaw and Dance, 2004; Rosenbauer and Thomas, 2010). In general, the kinetics of mineral trapping are believed to be comparatively slow (hundreds to thousands of years) but mineral trapping is considered the safest and most permanent mechanism to store CO_2 underground (Bergman and Winter, 1995; Garcia et al., 2010; IPCC, 2005; Reichle et al., 1999; Rosenbauer and Thomas, 2010). To date, studies have focused mainly on Ca- Mg- and Fe^{II}-bearing phases in potential formation rocks to precipitate aqueous CO_2 as calcite ($CaCO_3$), magnesite ($MgCO_3$), siderite ($FeCO_3$), or ankerite ($CaFe(CO_3)_2$) (Bateman et al., 2005; Giammar et al., 2005; Kaszuba et al., 2003; Kelemen and Matter, 2008; Liu and Maroto-Valer, 2010; Pruess et al., 2001; Rosenbauer et al., 2005; Suto et al., 2007).

Fe^{III}-bearing sediments, such as red beds, have been proposed as a mineral trap for CO_2, provided that a reducing agent is available to convert Fe^{III} to Fe^{II}, and to subsequently precipitate CO_2 as siderite ($FeCO_3$). Sulfur dioxide (SO_2), a common component of the flue gas, could be used as the reductant and co-injected with CO_2 (Palandri and Kharaka, 2005; Palandri et al., 2005). Experimental studies examining CO_2–SO_2 gas mixtures trapping in minerals are few (Mandalaparty et al., 2009; Palandri et al., 2005; Summers et al., 2004). Only one has been found that targeted ferric iron-bearing formations as potential host repositories for underground CO_2 storage (Palandri et al., 2005). This novel concept of injecting CO_2–SO_2 flue gas into Fe^{III}-bearing saline aquifers could also be applied to a new range of technologies currently under study to develop integrated pollutant removal systems for coal combustion (Chiesa et al., 2005; IPCC, 2005).

Total iron in red sandstone and mudstones averages 1.7–3.5%. Free (extractable) iron in the ferric oxide pigment averages about 0.67% (Van Houten, 1973). In addition, Fe is a common impurity in other sedimentary minerals. Red beds and sedimentary iron ores are groups of iron-containing sediments where hematite (α-Fe_2O_3) and goethite (α-FeOOH) are the main iron-bearing minerals. Hematite is abundant in ancient red beds whereas goethite is

* Corresponding author. Present address: Instituto Nacional del Carbón (INCAR), CSIC, Apartado 73, 33080 Oviedo, Spain. Tel.: +34 985 11 90 90; fax: +34 985 29 76 62.
E-mail address: sgarcia@incar.csic.es (S. Garcia).

1750-5836/$ – see front matter © 2011 Elsevier Ltd. All rights reserved.
doi:10.1016/j.ijggc.2011.12.004

abundant in younger yellow-brown coloured deposits (Gualtieri and Venturelli, 1999). Therefore, the potential for sequestering CO_2 in Fe-bearing sediments is worthy of further investigation. In addition, Fe^{III}-bearing sediments, including red beds, are thick, porous, and have high permeability (Blatt, 1982). Moreover, they are widespread geographically, making them potential sites for underground CO_2 sequestration as carbonates.

Goethite (α-FeOOH), which is more soluble than hematite, likely reacts faster than iron oxides with CO_2–SO_2 gas mixtures (Palandri et al., 2005). It can be present as thin grain coatings with a large surface area in red beds. Thus, goethite is here evaluated as a potential mineral phase for trapping CO_2 so both minerals, hematite and goethite, can be compared as potential mineral traps.

Theoretical calculations with the computer program CHILLER are used herein to predict the equilibrium condition in a goethite–CO_2–SO_2-brine system at 150 °C and 300 bar. Pure goethite was used for the simulations in lieu of a rock more representative of a natural red bed, which would be composed primarily of quartz with minor goethite. It was important to determine first if the reaction of CO_2 with goethite was favoured, thermodynamically and kinetically, and to compare these results with previous studies with pure hematite (Palandri et al., 2005). Geochemical models are useful predictive tools in geochemical systems but are limited by available thermodynamic data and necessary assumptions. For example, the model used here does not account for absolute rates of mineral dissolution and precipitation, nor aqueous speciation. Models which account for kinetics do exist and could be used to account for these factors. However, CHILLER was utilized as the geochemical code to compare the modeling results obtained herein with those obtained for the hematite–CO_2–SO_2-brine system (Palandri et al., 2005). Based on the output of the model, a laboratory experiment was designed to assess whether reaction kinetics favour the predicted phases as well as the validity of the simulations.

2. Geochemical reactions

The reaction of CO_2–SO_2 gas mixtures with ferric iron and water is complex. The overall reaction results in the formation of iron carbonate and sulfuric acid (reaction (1) for hematite and (2) for goethite).

$$Fe_2O_3(\text{hematite}) + 2CO_2 + SO_2 + H_2O \leftrightarrow 2FeCO_3 (\text{siderite}) + H_2SO_4 \quad (1)$$

$$2FeOOH(\text{goethite}) + 2CO_2 + SO_2 \leftrightarrow 2FeCO_3 + H_2SO_4 \quad (2)$$

The first step in reactions (1) and (2) is the dissolution and subsequent dissociation and disproportionation of the gases to their respective aqueous forms: HCO_3^-,CO_3^{2-}, H_2CO_3, HS^-, SO_4^{2-} and H_2S (reactions (3)–(9)).

$$4SO_2(g) + 4H_2O \leftrightarrow H_2S + 3H_2SO_4 \quad (3)$$

$$H_2S \leftrightarrow HS^- + H^+ \quad (4)$$

$$H_2SO_4 \leftrightarrow SO_4^{2-} + 2H^+ \quad (5)$$

$$CO_{2(g)} \leftrightarrow CO_{2(aq)} \quad (6)$$

$$CO_{2(aq)} + H_2O \leftrightarrow H_2CO_3 \quad (7)$$

$$H_2CO_3 \leftrightarrow HCO_3^- + H^+ \quad (8)$$

$$HCO_3^- \leftrightarrow CO_3^{2-} + H^+ \quad (9)$$

After these initial steps, dissolved sulfide can reduce Fe^{III} to Fe^{II} as sulfide is oxidized to sulfate (reaction (10)), and making Fe^{II} available for precipitation as iron carbonate, i.e. siderite (reaction (11)).

$$8Fe^{3+} + HS^- + 4H_2O \leftrightarrow 8Fe^{2+} + SO_4^{2-} + 9H^+ \quad (10)$$

$$H_2CO_3 + Fe^{2+} \leftrightarrow FeCO_3 + 2H^+ \quad (11)$$

Other possible reactions that can remove sulfide from the system include the precipitation of iron-sulfide minerals such as pyrite (reaction (12)).

$$4Fe^{2+} + SO_4^{2-} + 7HS^- + H^+ \leftrightarrow 4FeS_2(\text{pyrite}) + 4H_2O \quad (12)$$

If a sink does not exist to remove sulfide by oxidation to sulfate or by precipitation in iron-sulfide minerals, then sulfate and sulfide derived from the SO_2 disproportionation reaction may react to precipitate native sulfur (reaction (13)) in the system.

$$3H_2S + H_2SO_4 \leftrightarrow 4S(\text{native}) + 4H_2O \quad (13)$$

3. Methods

3.1. Modeling methods

Two thermodynamic simulations were computed at 150 °C and 300 bar to model the system containing goethite, CO_2–SO_2 gas mixtures and a 1.0 m NaCl, ±0.5 m NaOH brine. The only difference between the two simulations was the presence or absence of NaOH, which generates alkalinity and the capability to neutralize acid. The simulation with NaOH aimed to mimic the natural mineral buffering of pH as the addition of NaOH increases the bicarbonate content by an amount equal to the OH^- concentration. Hence, the bicarbonate–carbonate equilibria (reaction (9)) is shifted towards carbonate which promotes siderite precipitation by increasing its saturation index. Natural minerals (carbonates, bicarbonates, silicates, phosphates, etc.), which provide buffering capacity, could also have been used in the model. However, NaOH was used for comparison purposes with previous work with hematite (Palandri et al., 2005). The theoretical results from the model were then compared to experimentally derived results on the same system.

The computer program CHILLER was used for modeling equilibria in the aqueous system. For a given temperature (T), pressure (P) and total composition (x) of a chemical system, CHILLER computes multi-component heterogeneous chemical equilibria among solids, gases and an aqueous phase (Reed and Spycher, 2006). The aqueous activity coefficients are computed using the extended Debye-Hückel equation of Helgeson and co-workers (Helgeson et al., 1981), as modified by Tanger and Helgeson (1988) and gas fugacities for CO_2, H_2O, CH_4, H_2, and mixtures of CO_2, H_2O and CH_4, using a virial equation as discussed by Spycher and Reed (1988). The accurate calculation of aqueous activity coefficients in the method requires that NaCl be the dominant solute at ionic strength greater than ~1 m and that the total salinity not exceed ~3 m (Palandri and Reed, 2004). SOLTHERM is the thermodynamic database of equilibrium constants for minerals, gases and aqueous species used by CHILLER. Equilibrium constants were calculated using the software package SUPCRT92 (Johnson et al., 1992), modified with a four term heat capacity regression equation, to use an internally consistent mineral thermodynamic dataset for silicates, oxides, hydroxides, carbonates and gases from Holland and Powell (1998); gases and non-silicate minerals that do not appear in the Holland and Powell database, and aqueous species are taken from Shock et al. (Shock et al., 1997). Ideality is assumed for SO_2 gas due to lack of thermodynamic data to compute its fugacity coefficients. This assumption is considered to be valid because SO_2 gas is very soluble in aqueous fluids so that its content in the gas phase is negligible.

In the simulation with a pH buffer, 150 ml of a 1.0 m NaCl brine is first equilibrated with a 0.5 m NaOH solution at 300 bar, followed

by heating to 150 °C, and further equilibration with 10 g of goethite. In the simulation without NaOH, 150 ml of NaCl (1.0 m) were equilibrated with 10 g of goethite. Equilibration with excess CO_2 (14 g) was performed next in both instances (with and without NaOH) and incremental addition of SO_2 (up to 40 g) completed the simulations. Equilibrium is computed after each increment of SO_2 gas added to the system. Only the SO_2 addition portion of the calculation is presented in the results discussed below. We then utilized the theoretical results to establish the experimental conditions.

3.2. Experimental methods

A natural goethite sample from El Paso County (Colorado) was purchased from Ward's Natural Science Establishment. This parent material was crushed, ground and sieved to segregate a 75–150 μm size fraction. The XRD spectra for the goethite sample confirmed the presence of the iron oxyhydroxide only.

3.2.1. Experimental apparatus and set-up

A flexible Au–Ti reaction cell was loaded with 10 g of goethite (75–150 μm) and 154.5 g of nitrogen-purged 1.0 m NaCl, 0.5 m NaOH solution. The reaction cell was sealed and loaded into an autoclave. The autoclave was then secured to a rocking furnace that oscillates vertically 180° on axis. The furnace and autoclave containing the reaction cell are rotated (1) to maintain temperature stability and homogeneity and (2) to ensure that the reactants are well mixed and thus enhance reaction kinetics. The pressure vessel was pressurized to 200 bar by adding water to the annular space around the reaction vessel via a compressed air-driven hydraulic pump, causing the reaction cell to slowly collapse. 14 g of CO_2 (15.3 ml at 25 °C and 200 bar) were then added through the sampling valve of the reaction cell with a syringe pump (ISCO Corp.) to super-saturation; the assembly was heated to 150 °C and the pressure adjusted to 300 bar by withdrawing water from the autoclave. 3 g of SO_2 (3.8 ml at 25 °C and 300 bar) were added to the experiment, again through the sampling valve of the reaction cell, via syringe pump. This SO_2 amount is derived from model results (which are explained in detailed below) and was chosen because it maximizes siderite precipitation. Temperature was maintained by a proportional controller and measured with a type K thermocouple calibrated to a platinum resistance temperature detector (RTD). Pressure was measured with analogue gauges and digital transducers (Heise).

At the end of the experiment, the pressure was lowered to 200 bar and the reactor was cooled to 80 °C. When temperature reached 80 °C, the reactor was vented again and placed in a water bath for quenching and venting of the remaining gas inside.

3.2.2. Sampling and analytical methods

Aqueous samples (approximately 2.5 ml) were withdrawn periodically during the experiment for chemical analyses to determine changes in fluid composition over time. The pressure in the pressure vessel was maintained while sampling via the hydraulic pump that adds enough fluid to accommodate the volume of sample taken. Sampling and pressurizing of the pressure vessel can be performed simultaneously so that sampling is both an isothermal and isobaric process. Aqueous samples were analyzed immediately after sampling for total dissolved inorganic carbon by coulometric titration, fluid salinity by its refractive index measurement, fluid pH at ambient temperature and dissolved ferrous and total iron by spectrophotometry (ferrozine method). Ferric iron is determined from the difference between the total and ferrous iron values. A UV–VIS spectrophotometer from Shimadzu with an accuracy of ±1 nm was employed for the measurements. Aliquots for dissolved anions were preserved and analyzed in batch mode by ion chromatography at the end of the experiment. A Dionex (model DX500) Ion Chromatograph with a detection limit of 20 ppb was used for the analyses.

After completion of the experiment the solution was filtered with a Buchner funnel and cellulose filters (Whatman fine) to separate and recover the solids. Next, the reaction cell was rinsed with distilled water that was also filtered and collected until all the solids were recovered. Aliquots were collected from the filtrates to measure the iron in solution due to quench effects of retrograde dissolution. Residual solids were dried overnight, weighed and saved for analyses.

The mineralogy of the starting material and reaction products was determined by a bulk technique, thermal analysis (TGA), and a surface technique, X-ray photoelectron analysis (XPS). The latter provides qualitative and quantitative information on the surface of the samples (approximately the top 10 nm) and can be very useful for looking for compositional changes at mineral surfaces after the reactions of interest (Watts and Wolstenholme, 2003). Data from more conventional analytical methods such as X-ray diffraction (XRD) or Scanning Electron Microscopy (SEM) did not add any significant results. TGA analyses were recorded at atmospheric pressure in a Q500 Thermogravimetric Analyzer (with a sensitivity of 0.1 μg) from TA Instruments. Samples (~20–40 mg) placed in Pt crucibles were first equilibrated at 30 °C and then heated under a N_2 atmosphere at 10 °C/min from 30 to 900 °C, with one stop at 105 °C for 15 min. Samples for XPS were run under the charge neutralization conditions (Kratos AXIS Nove charge neutralization system) and charge correction was normally achieved by setting the aliphatic carbon peak to 285.0 eV (due to adventitious carbon surface contamination).

4. Reaction of goethite with CO_2, and SO_2, in a NaCl brine at 150 °C and 300 bar – Results and discussion

4.1. Modeling results

Fig. 1 shows the equilibrium mineral/gas phase assemblage and fluid composition for increasing amounts of SO_2 gas added for the simulations with (Fig. 1a and c) and without pH buffering (Fig. 1b and d). In the simulation with the pH buffer, the computed pH of the fluid upon equilibration with NaOH is 13.4 compared to 5.8 for the case without NaOH addition. Equilibration of the fluid with goethite at the reaction conditions yields a pH of 10.9 and 5.8 for buffered and non-buffered cases respectively. Further equilibration with excess supercritical CO_2 yields a pH of 5.9 and 3.3 for the above cases. Finally, simulations are completed with incremental SO_2 addition (only this part of the calculation is presented in Fig. 1) and the results are discussed below.

For the buffered case, the computed equilibrium mineral/gas phase assemblage (Fig. 1a) indicates siderite is the stable phase over a wide range of SO_2 gas added, from −4.0 (off-scale left) to 1.06 log g (from 0.1 mg to 11.5 g). Further addition of SO_2 yields dissolution of siderite and, after all of the goethite has dissolved pyrite precipitates. With further SO_2 addition, native sulfur replaces pyrite.

At very small amounts of SO_2 added, the pH remains nearly constant (Fig. 1c), buffered mostly by HCO_3^- and also by goethite dissolution, which consumes H^+. Both the addition of SO_2 and siderite precipitation, generate acidity (reactions (3) and (11) respectively). After ~0.25 g (−0.6 log g) of SO_2 added, the pH begins to decrease because the amount of H^+ generated becomes greater than that consumed by goethite dissolution. The slope of the pH curve decreases as siderite begins to dissolve consuming H^+, followed by a further steep decrease when pyrite precipitates, i.e. this reaction (12) consumes H^+ but not at as high a proportion as siderite dissolution. The formation of native sulfur causes a plateau in pH until pyrite dissolves completely, after which the pH declines again

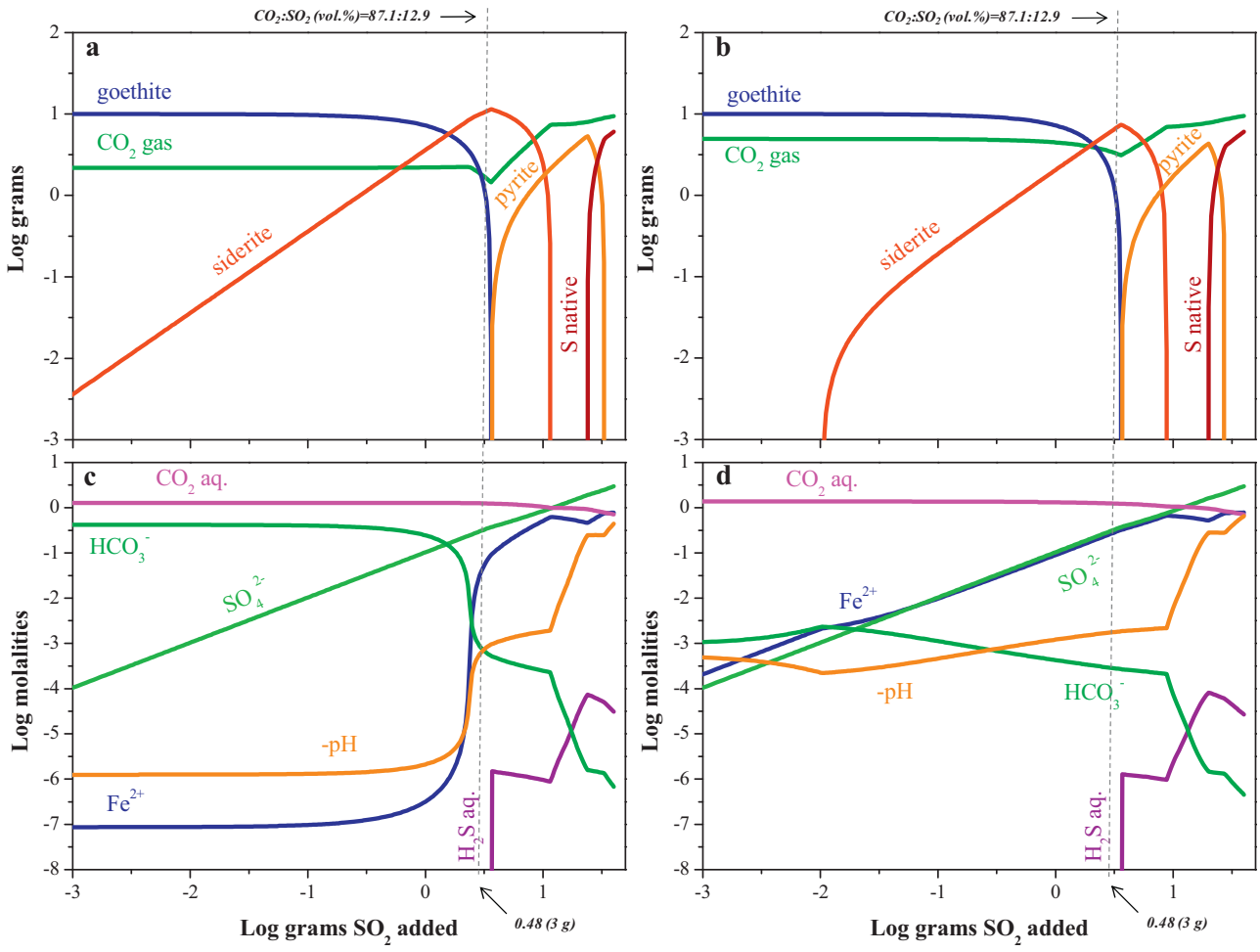

Fig. 1. Results from simulations at 150 °C and 300 bar of the CO_2–SO_2 reaction with 10 g of goethite in 154.5 g of 1.0 m NaCl, 0.5 m NaOH brine using 14 g (excess) CO_2: buffered case (a and c) and un-buffered case (b and d). Mineral/gas phase assemblage is depicted in top graphs (a and b) and fluid composition in bottom ones (c and d). The vertical line indicates the amount of SO_2 chosen for the experimental case, 0.48 log g (3 g) of SO_2 added (i.e. a CO_2:SO_2 composition of 87.1:12.9 vol.%).

in response to the precipitation of native sulfur as the only active process.

Total dissolved iron concentration, present mainly as Fe^{2+}, $FeCl^+$, $FeCl_2$, FeO, $FeOH^+$ and $FeSO_4$, remains almost constant and very low (~10^{-7} mol/kg solvent) until the pH becomes acidic (~3.0) (Fig. 1c). Total dissolved sulfate, mostly as SO_4^{2-}, $FeSO_4$, $NaSO_4^-$ and HSO_4^-, increases steadily over the course of the simulation due to the addition of gas. SO_2 gas disproportionates into sulfate and sulfide and only traces of thiosulfate and sulfite. The concentration of reduced S species, H_2S, HS^-, S^{2-}, SO_3^{2-}, $S_2O_3^{2-}$, are very low until goethite completely dissolves, increasing in response to SO_2 addition (Fig. 2). These concentrations level off when pyrite becomes the stable phase because S is being incorporated into pyrite rather than remaining dissolved in the fluid (reaction (12)).

Trends of bicarbonate concentration and pH follow an inverse relation (Fig. 1c), reflecting how a closed carbonate system is strongly linked to the composition and pH of the brine (Stumm and Morgan, 1996).

The simulations are very similar for the pH buffered and non-buffered case. Differences include a much lower initial pH and a higher dissolved Fe^{II} concentration in the simulation without a pH buffer (Fig. 1c and d) and consequently less siderite precipitates (Fig. 1b). Here, total dissolved Fe^{II} concentration increases steadily over the course of the simulation, i.e. with SO_2 addition. Brine pH increases initially due to goethite dissolution, which consumes H^+, to a point where siderite starts to precipitate (Fig. 1d). From that point forward, pH decreases due to more carbonic acid dissociating into bicarbonate and carbonate ions when siderite precipitates, which generates acidity. A further decrease is observed when pyrite precipitates and finally, S native formation consumes acidity so that the pH levels off until it decreases again due to the SO_2 addition. Again the bicarbonate concentration and pH trends follow an inverse relation in both simulations due to their strong link in a closed system.

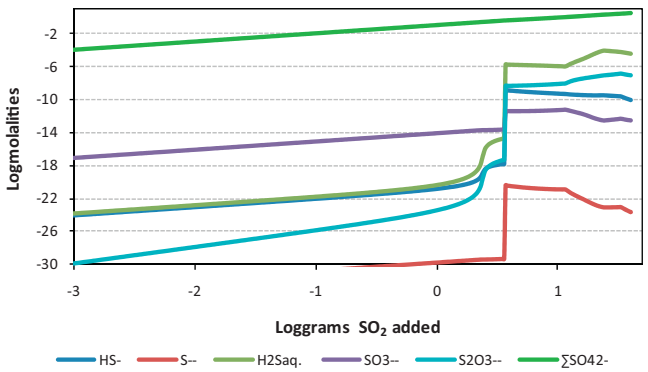

Fig. 2. Equilibrium sulfur species concentration for the buffered case model with goethite at 150 °C and 300 bar.

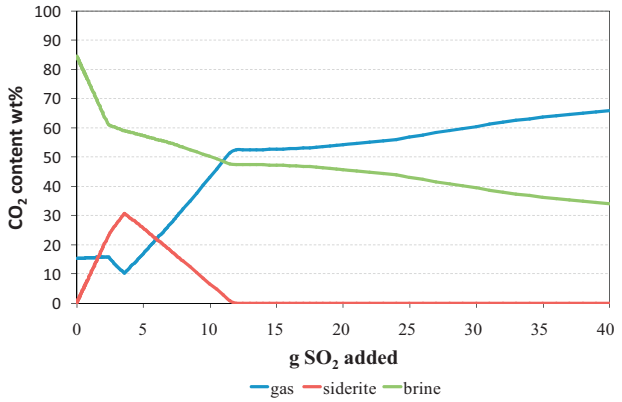

Fig. 3. Carbon partitioning in the system for the pH-buffered simulation at 150 °C and 300 bar.

Siderite precipitates over a wider range of added SO_2 in the system with a pH buffer; hence, this case was selected for the experimental run, aiming to observe the desired carbonate product, siderite, on the time scale of a laboratory experiment. The vertical line in Fig. 1 indicates the amount of SO_2 chosen for the experimental case, 0.48 log g (3 g) of SO_2 added, because at that point the amount of precipitated siderite is close to its maximum. Beyond this point, further addition of SO_2 would yield pyrite and, in a very acidic environment, native sulfur. The equilibrium mineral assemblage for 3 g of SO_2 added should consist only of goethite and siderite, with a conversion of 78.2% of the Fe present in the goethite into siderite and 0.39 g of CO_2 sequestered in siderite per g of goethite.

The mass balance for the total carbon in the system showing how it partitions among the different phases (gas, siderite and brine) can be seen in Fig. 3, where $\sum CO_2$ denotes the total aqueous carbonate concentration and is defined as follows:

$$\sum CO_2 = [H_2CO_3] + [HCO_3^-] + [CO_3^{2-}]$$

Siderite precipitation reaches its maximum mass at a CO_2/SO_2 gas composition of ~80/20 wt% (corresponding to 3.6 g of SO_2 added), where ~30% of the CO_2 is contained in the carbonate. Even at that inflection point (CO_2/SO_2 = 80/20 wt%), the fluid contains about 2 times (~60%) the amount of CO_2 present in the solid in a given volume of brine and solid. For a gas stream containing 12.9% SO_2, which corresponds to 3 g of SO_2 added (experimental case), 60% of the CO_2 is trapped in brine followed by trapping in carbonate form (27.2%), i.e. siderite, while remaining CO_2 exists as a supercritical gas phase (12.7%).

Theoretical equilibrium calculations performed with CHILLER do not account for kinetics. Therefore, the precipitation and persistence of metastable phases are always a possibility even if the final products of a chemical reaction are favoured thermodynamically.

4.2. Experimental results

4.2.1. Analysis of fluid chemistry

Fluid samples were taken daily near the beginning of the experiment, and then at increasing longer intervals to monitor changes in the fluid chemistry and approach to steady-state (Table 1). Total and ferrous iron concentrations were less than 2 ppm during the entire duration of the experiment but much elevated in the quench fluid (Table 1), likely due to the dissolution of siderite during the quench. Siderite, like most carbonates, has a retrograde solubility and is less soluble and more stable at elevated temperatures (Greenberg and Tomson, 1992; Sun et al., 2009). Dissolved iron concentration in the rinse fluid was almost three times higher than in the quench fluid indicating that the rinsing process dissolved an iron-containing phase; iron sulfate shows a high solubility in water at atmospheric pressure and temperature (25.6 g/100 g H_2O) (Lide, 1999). However, an iron sulfate precipitate is unlikely and dissolved iron might be coming from some siderite dissolving in the rinse fluid (Sun et al., 2009).

Changes in pH early in the experiment (a sharp decrease follows a steep increase) suggest the formation of a pH dependent precipitate. It is important to point out that pH values are maxima due to CO_2 out degassing during measurement. The observed decrease in pH could be due to precipitation of siderite (reaction (11)), which consumes carbonate ions and causes a re-speciation of dissolved carbonate. Precipitation of other phases involving H^+ production such as iron sulfide (reaction (14)) could also contribute to the observed pH drop.

$$Fe^{2+} + HS^- \leftrightarrow FeS(\text{amorphous}) + H^+ \quad (14)$$

Total dissolved CO_2 should remain approximately constant over the course of the experiment because CO_2 is present in excess as a separate supercritical phase. Some changes in CO_2 concentration were observed early in the experiment due to dissolution, with an initial sharp increase followed by a decrease to a constant value for the rest of the experiment (Table 1). The refractive index, a measure of total salinity, remained constant throughout the experiment.

Disproportionation of SO_2 yielded high concentrations of sulfate and thiosulfate (Table 1) and minor sulfite. The latter could not be quantified because it is rapidly oxidized to sulfate; this process was observed also by Palandri and co-workers in a similar experiment (Palandri et al., 2005). Palandri et al. (2005) inferred a reaction between sulfite and sulfide producing thiosulfate with remnant sulfite. No significant changes are observed in sulfate and thiosulfate concentrations over the course of the experiment except for a slightly decreasing trend in sulfate concentration towards the end of the experiment. This might be the result of precipitation of S-bearing phases whose precipitation consume sulfate such as pyrite and sulfur (reactions (12) and (13) respectively). The odour of sulfide was not detected throughout the experiment in any of the fluid samples nor upon opening the reaction cell.

The experimental values obtained for total sulfate and thiosulfate concentrations differ significantly from those predicted by the model: the concentration of sulfate is only half the expected given the 3 g of SO_2 used; the presence of thiosulfate in solution, with a concentration that is lower than 2000 ppm over the entire duration of the experiment, is attributed to the aforementioned reaction between sulfite and sulfide. However, in the model, the disproportionation reaction of SO_2 only yielded sulfate and sulfide and negligible amounts of thiosulfate and sulfite. Likewise, the dissolved iron concentration in the experiment is very low (less than 2 ppm) compared to that predicted by the model (~2000 ppm). It seems that goethite dissolved more slowly in the experiment than predicted by the model; hence, kinetics play an important role in this system. Discrepancies between experimental and modeling results could be partly due to the program not accounting for kinetics. And, although the calculations in the model are based on a solid thermodynamic framework, the modeling work could be in error due to its lack of speciation.

4.2.2. Solid samples analyses

Analysis of the reaction products by XPS revealed that the solid surfaces had undergone significant alteration and confirmed the formation of carbonate precipitates. Each sample was analyzed in quadruplicate, targeting four different sites within the sample.

First, a wide scan was performed to identify the elements on the sample surface according to their binding energies (BE). Areas under peaks intensities were used to calculate concentrations of the elements as percentages of total intensity. Significant changes are seen in the surface elemental content of the un-reacted, reacted,

Table 1
Fluid composition and pH over the course of the experiment: dissolved sulfur (sulfate and thiosulfate), total dissolved CO_2, dissolved iron (total iron and ferrous iron) and fluid pH.

Reaction time (h)	$[SO_4^{2-}]$ (ppm)	$[S_2O_3^{2-}]$ (ppm)	ΣCO_2 aq. (wt.%)	$[Fe^{2+}]$ (ppm)	[Fe total] (ppm)	pH
2	14374.2	1272.0	2.6	0.0	0.0	6.6
44	12489.8	710.8	6.9	0.7	1.0	6.9
63	13845.9	652.7	4.1	0.0	0.0	7.2
112	12885.3	770.6	5.1	0.0	0.0	6.7
232	13533.6	393.8	5.7	0.0	0.0	6.6
280	12010.3	305.6	4.7	0.5	0.6	6.6
329	14651.7	1000.0	5.1	0.0	0.0	6.7
399	13826.5	861.1	4.9	0.5	0.6	6.6
448	13677.0	1000.0	5.2	0.0	0.0	6.6
497	13429.5	1416.7	4.7	0.0	0.0	6.7
566	11984.0	1972.2	4.8	0.5	0.6	6.5
571[a]	11292.0	1000.0	–	12.9	13.2	7.1
571[b]	–	–	–	34.7	35.6	–

[a] Quench fluid.
[b] Rinsed fluid.

and rinse-reacted samples (Table 2). The sodium content of the solid increased as a result of the reaction and decreased very significantly upon the rinsing process (Table 2); the increase in sodium content could result from incomplete rinsing of the brine from the reacted sample so chloride was also analyzed to determine if it behaved in a similar way to sodium. It can be seen in Table 2 that chloride atomic %concentration was lower in the reacted sample than in the un-reacted one, indicating that the increase in sodium can not be attributed entirely to residual salt. Rather, the sodium appears to be incorporated and/or adsorbed onto the iron oxyhydroxide. Sulfur, silicon, aluminium and fluoride content decreased as a result of the reaction, mainly due to dissolution from the solids. The carbon content also increased after the reaction and decreased slightly with the rinsing process.

A decreased atom %concentration of sodium, carbon, chloride and sulfur is observed in the rinsed sample with respect to the reacted sample (Table 2). Sodium content decrease (3.6%) was almost the same as the sulfur, chloride and carbon combined content decrease (3.7%). Hence, S, Cl and C-containing sodium compounds could have been present and/or adsorbed and later dissolved with the rinsing process. Phases like NaCl, Na_2CO_3, Na_2SO_4/$Na_2S_2O_3$ and $FeSO_4$ are very unlikely to precipitate either under experimental conditions or when quenching the experiment because most of these compounds are very soluble (Lide, 1999). The surface iron content increased in the rinsed sample compared to the reacted sample but this is an artifact of dilution by the decreased content of other elements, making the iron content higher in percentage.

Additionally, a high resolution XPS spectra for the carbon element (C1s) (Fig. 4) was obtained in order to elucidate the nature of the carbon present on the surface of the samples. The peak at 285.0 eV is typically assigned to adventitious (aliphatic) carbon found in all samples exposed to the atmosphere. The C1s region was peak-fit using four Gaussian–Lorentzian synthetic components. The solid black line represents experimental data and the total calculated fit is shown in grey with circular markers. The other curves represent components used to curve fit the spectra. It can be seen that a new peak centred at 289.6 eV is formed after the reaction, which corresponds to carbonate formation as predicted by geochemical modeling. Reference BE values for the carbonate peak in siderite and sodium carbonate are 289.8 and 289.4 eV respectively, as determined by XPS analysis of reference compounds (Fig. 5). The BE for the peak related to carbonate carbon atoms in the reacted sample is in between the values for the iron and sodium carbonates; this could indicate the presence of both carbonates although a sodium carbonate precipitate is very unlikely. The BE of the carbonate peak in the reacted + rinsed sample shifts to a higher value (289.8 eV) which is characteristic of siderite (Fig. 4). Thus, siderite is the only carbonate present in the rinsed sample.

In the bulk analyses, thermal decomposition of un-reacted, reacted and rinse-reacted samples revealed a small percentage of weight loss (~0.8%) at the decomposition temperature of siderite, ca. 400 °C (Bayliss and Warne, 1972; Kotra et al., 1982), in the rinse-reacted sample (Fig. 6). This observation is in good agreement with results from XPS analyses, indicating that siderite was the only carbonate phase present in the rinse-reacted solid.

An estimation of the siderite content of the final solid (rinse-reacted sample) can be calculated according to reaction (15) below:

$$FeCO_3 \xrightarrow{\Delta} FeO + CO_2 \quad (15)$$

Assuming all the remaining siderite decomposed in the TGA analysis, 2.1% of iron carbonate was present in the rinse-reacted solid.

Residual solids after the experiment were 9.1 g so 8.7% of weight loss was observed versus the 18.8% weight uptake predicted by geochemical modeling. Experimentally, conversion of Fe from goethite into siderite was 1.5%, which differs significantly from the predicted equilibrium case (78.2%). Thereby, only 76 mg of CO_2 were sequestered in siderite per 10 g of sample instead of predicted 3.9 g. It is important pointing out that this experimental value (76 mg of CO_2 in $FeCO_3$/10 g goethite) is an underestimate because some of the siderite that precipitated over the course of the experiment might have dissolved in the quenched and rinsed fluid. It is also likely that the reaction did not go to completion within the 24 day timeframe of the experiment.

Table 2
Results of XPS analysis of goethite in atomic relative percentage. Terms in brackets next to the element symbols indicate the photoelectron emission used in the analysis. Values shown have been computed as the average value of four different measurements.

Sample	Na [1s]	Fe [2p]	O [1s]	C [1s]	Cl [2p]	S [2p]	Si [2p]	Al [2p]	F [1s]
Unreacted	3.1 ± 0.3	7.4 ± 3.6	47.7 ± 3.9	22.6 ± 3.9	1.6 ± 0.3	1.5 ± 0.1	4.3 ± 1.0	1.4 ± 0.0	10.4 ± 1.0
Reacted	5.3 ± 0.3	9.7 ± 0.2	48.9 ± 1.9	31.7 ± 0.4	1.0 ± 0.1	0.8 ± 0.0	1.7 ± 0.4	1.0 ± 0.3	0.0 ± 0.0
Reacted + rinsed	1.7 ± 0.3	11.1 ± 0.5	53.7 ± 0.9	29.4 ± 0.3	0.2 ± 0.0	0.2 ± 0.2	2.5 ± 0.4	1.2 ± 0.2	0.0 ± 0.0

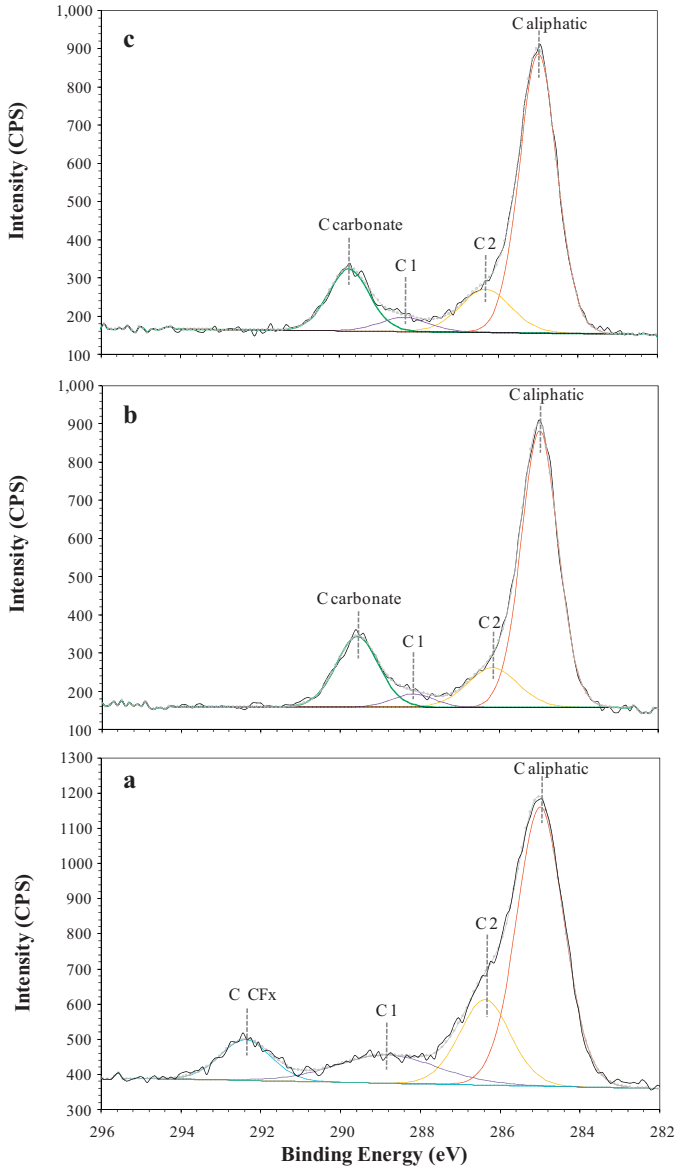

Fig. 4. High resolution XPS in the C1s region for the un-reacted (a), reacted (b) and reacted + rinsed samples (c).

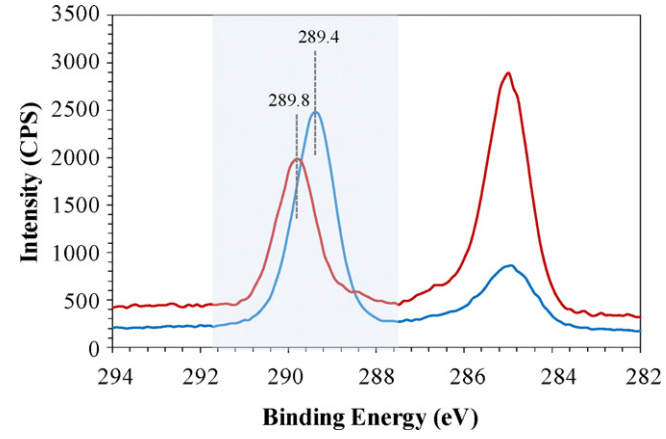

Fig. 5. XPS C1s spectra of standard iron carbonate, i.e. siderite (red line), and sodium carbonate (blue line). (For interpretation of the references to color in this figure legend, the reader is referred to the web version of this article.)

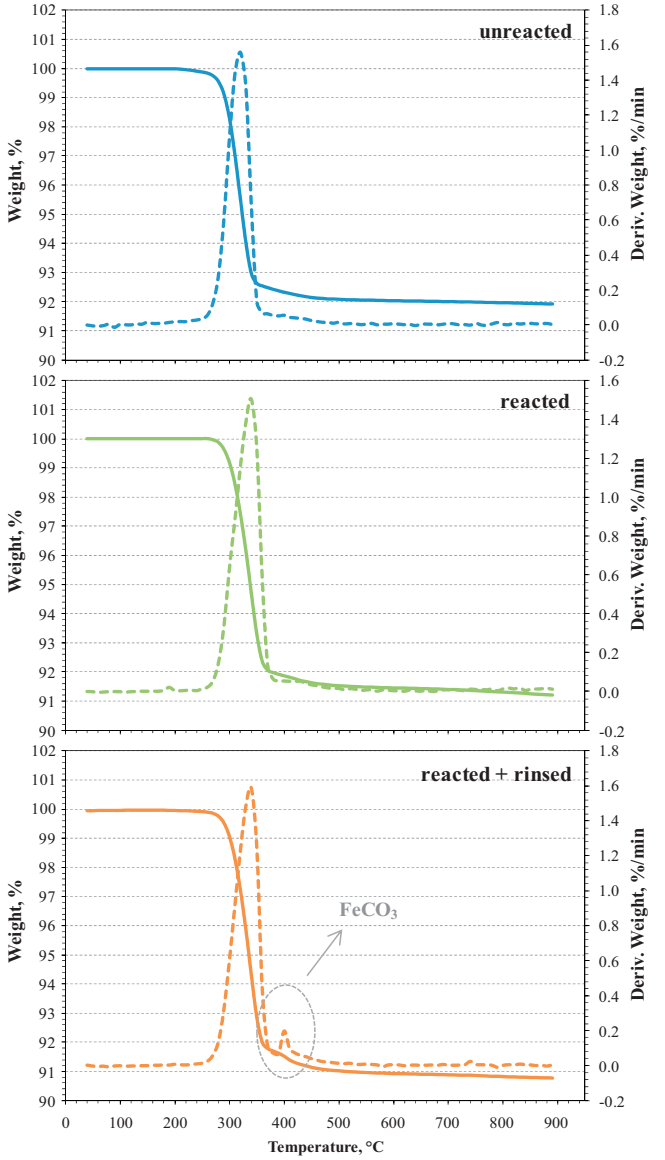

Fig. 6. TGA curves of unreacted, reacted and rinse-reacted goethite samples. Dashed lines correspond to derivative weight curves.

5. Discussion and implication for the geological storage of CO_2

In this work, siderite precipitation was observed within shorter reaction times (~576 h) than in previous experimental work with hematite (~611 h) (Palandri et al., 2005). In the latter, two other metastable phases precipitated early (~17 h) in the experiment, pyrite and S, which did not precipitate in the present experiment with goethite. Quantitatively, 76 mg of CO_2 were sequestered in siderite per 10 g of goethite, i.e. 2.4% by volume of siderite is present in the reaction products, versus the estimated 0.1–0.5% in the experiment with hematite (Palandri et al., 2005). Therefore it appears that the reactivity is higher for goethite than hematite. Not only did siderite precipitate faster, but also the total amount of CO_2 trapped in mineral form was much higher for goethite than for hematite. Formations containing α-FeOOH (goethite) minerals should be then better host repositories for underground CO_2 sequestration than those containing hematite (α-Fe_2O_3). The reactivity of goethite is in good agreement with previous studies (dos Santos Afonso and Stumm, 1992) that concluded goethite

dissolution was faster than hematite. The dissolution of iron oxides can be visualized as the breaking of surface ionic bonds, so the higher reactivity of goethite is related to the nature of its hydrogen bonds, which are easier to break than the metal–oxygen–metal bonds that characterize the hematite structure.

It is also important to note the potential injection depth because hematite and goethite stability depends on different conditions of temperature, pressure and salinity (Bischoff, 1969). Although there is some degree of uncertainty in the equilibrium temperature between hematite and goethite in pure water at atmospheric pressure (Bischoff, 1969; Smith and Kidd, 1949), 130 °C is being taken as a valid approximation. The stability field of goethite is also enhanced with increasing pressures and decreasing salinities (Bischoff, 1969). Hence, in injections at depths >5 km, given an average geothermal gradient (25 °C/km), goethite will not be found in the host reservoir rock. However, such deep injections are highly unlikely in a full-scale operation due to the high drilling and operational costs involved.

Based only on molar volume changes and assuming 100% pure hematite and goethite-containing reservoirs ($\tilde{V}_{hematite}$ = 30.27 and $\tilde{V}_{goethite}$ = 20.82 cm^3/mol (Weast, 1984)), their complete alteration to thermodynamically stable siderite ($\tilde{V}_{siderite}$ = 29.38 cm^3/mol (Weast, 1984)) will increase the mineral volume 95 and 41% respectively. The porosity reduction because of the above increase would greatly affect the dynamics of the system, and if the porosity loss occurs in the pore throats, permeability will be reduced as well. In this regard, goethite would be a better host reservoir than hematite, since the volume increase is about half that for hematite. Even though predictions can be made on what might happen to porosity in real systems, actual numbers could only be calculated when knowing the in situ host rock composition along with its initial porosity.

Theoretical and experimental work conducted herein show that thin grain coatings of goethite, such as those in red beds, contain ferric iron in quantities that can scrub all the SO_2 contained in a flue gas stream. The flue gas derived from the combustion of fossil fuel typically contains between 0.15 and 2 vol.% of SO_2, when deliberately recovered and incorporated with CO_2 in the injectate (Apps, 2006). However, most CO_2 will remain in a supercritical or dissolved phase instead of being trapped as siderite. Depending on the water-rock ratio, i.e. goethite might be all used up, and CO_2:SO_2 gas composition, an insufficient SO_2 amount might be present in the gas stream to reduce all the Fe present in goethite and trap all the CO_2 in siderite. Hence, in the above cases, either the targeted sediments contain additional divalent metals such as Ca or Mg, or additional sulfur-bearing gas is added to the waste gas stream to effectively trap CO_2 in carbonate form.

6. Conclusions

The objective of this work was to evaluate iron oxyhydroxide, goethite (α-FeOOH), as a potential mineral that could react with CO_2 and store it by mineral trapping, when a mixture of CO_2–SO_2 flue gas is injected into saline aquifers. Results obtained in a 24 day experiment are consistent with the modeling simulation that predicted an iron carbonate should precipitate in a goethite–CO_2–SO_2-brine system at 150 °C and 300 bar. Analyses of residual solids from experiments under the same conditions are in agreement with changes in fluid composition. XPS analyses largely confirmed changes on the mineral surfaces consistent with the formation of siderite. Bulk solid thermal analysis were consistent with the XPS analyses. Calculations based on TGA curves showed 76 mg of CO_2 were sequestered in iron carbonate per 10 g of goethite.

Goethite-containing saline reservoirs are a potential option to trap geochemically CO_2–SO_2 gas mixtures, and they are more efficient than hematite-containing reservoirs. The benefits of targeting goethite deposits are twofold: the mineral trapping process is faster with goethite and the expected consequences on hydrologic properties of the aquifer are more favorable. In this work SO_2, which specifically may be acceptable/allowed under future CO_2 capture regulations, is a potential reductant for mineral trapping of CO_2 by Fe and could be co-injected with CO_2 instead of separated from the gas stream at great expense.

Acknowledgments

The financial support of the Centre for Innovation in Carbon Capture and Storage (CICCS) through the Engineering and Physical Sciences Research Council, EPSRC (EP/F012098/1), and the University of Nottingham Business-Engineering and Science Travel Scholarships (BESTS) Program is gratefully acknowledged. The authors also thank Junfeng Qin, Larry Miller and Gil Ambats at USGS and Ignacio Villar at the University of Nottingham for their help and assistance in the lab, IC analyses, spectrophotometric and XPS analyses respectively. Thanks are also due to James Bischoff and Burt Thomas for suggestions and comments to improve this manuscript.

References

Apps, J.A., 2006. A Review of Hazardous Chemical Species Associated with CO_2 Capture from Coal-fired Power Plants and their Potential Fate During CO_2 Geological Storage. Lawrence Berkeley National Laboratory, Berkeley, CA, USA.

Bachu, S., Adams, J.J., 2003. Sequestration of CO_2 in geological media in response to climate change: capacity of deep saline aquifers to sequester CO_2 in solution. Energy Conversion and Management 44, 3151–3175.

Bateman, K., Turner, G., Pearce, J.M., Noy, D.J., Birchall, D., Rochelle, C.A., 2005. Large-scale column experiment: study of CO_2 porewater, rock reactions and model test case. Oil & Gas Science and Technology 60, 161–175.

Bayliss, P., Warne, S.S.J., 1972. Differential thermal analysis of siderite-kaolinite mixtures. American Mineralogist 57, 960–966.

Bergman, P.D., Winter, E.M., 1995. Disposal of carbon dioxide in aquifers in the U.S. Energy Conversion and Management 36, 523–526.

Bischoff, J.L., 1969. Goethite-hematite stability relations with relevance to sea water and the Red Sea brine system. In: Degens, E.T., Ross, D.A. (Eds.), Hot Brines and Recent Heavy Metal Deposits in the Red Sea – A Geochemical and Geophysical Account. Springer-Verlag, Berlin, pp. 402–406.

Blatt, H., 1982. Sedimentary Petrology. Freeman, W.H., Oxford.

Bradshaw, J., Dance, T., 2004. Mapping geological storage prospectivity of CO_2 for the world's sedimentary basins and regional source to sink matching. In: Rubin, E.S., Keith, D.W., Gilboy, C.F. (Eds.), 7th Intenational Conference on Greenhouse Gas Technologies (GHGT-7). Vancouver, Canada, pp. 583–592.

Chiesa, P., Consonni, S., Kreutz, T., Robert, W., 2005. Co-production of hydrogen, electricity and CO_2 from coal with commercially ready technology. Part A. Performance and emissions. International Journal of Hydrogen Energy 30, 747–767.

dos Santos Afonso, M., Stumm, W., 1992. Reductive dissolution of Iron (III) (hydr)oxides by hydrogen sulfide. Langmuir 8, 1671–1675.

Garcia, S., Kaminska, A., Maroto-Valer, M.M., 2010. Underground carbon dioxide storage in saline formations. Waste and Resource Management 163, 77–88.

Giammar, D.E., Bruant Jr., Peters, R.G.C.A., 2005. Forsterite dissolution and magnesite precipitation at conditions relevant for deep saline aquifer storage and sequestration of carbon dioxide. Chemical Geology 217, 257–276.

Greenberg, J., Tomson, M., 1992. Precipitation and dissolution kinetics and equilibria of aqueous ferrous carbonate vs temperature. Applied Geochemistry 7, 185–190.

Gualtieri, A.F., Venturelli, P., 1999. In sity study of the goethite-hematite phase transformation by real time synchrotron powder diffraction. American Mineralogist 84, 895–904.

Helgeson, H.C., Kirkham, D.H., Flowers, G.C., 1981. Theoretical prediction of the thermodynamic behavior of aqueous-electrolytes at high-pressures and temperatures. 4. Calculation of activity-coefficients, osmotic coefficients, and apparent molal and standard and relative partial molal properties to 600 °C and 5 kb. American Journal of Science 281, 1249–1516.

Holland, T.J.B., Powell, R., 1998. An internally consistent thermodynamic data set for phases of petrological interest. Journal of Metamorphic Geology 16, 309–343.

IPCC, 2005. IPCC special report on carbon dioxide capture and storage, in: Metz, B., Davidson, O., de Coninck, H.C., Loos, M., Meyer, L.A. (Eds). Prepared by Working Group III of Intergovernmental Panel on Climate Change, Cambridge, United Kingdom and New York, NY, USA, pp. 1–442.

Johnson, J.W., Oelkers, E.H., Helgeson, H.C., 1992. Supcrt92 – a software package for calculating the standard molal thermodynamic properties of minerals gases, aqueous species, and reactions from 1-bar to 5000-bar and 0-degrees-C to 1000-degrees-C. Computers & Geosciences 18, 899–947.

Kaszuba, J.P., Janecky, D.R., Snow, M.G., 2003. Carbon dioxide reaction processes in a model brine aquifer at 200 °C and 200 bars: implications for geologic sequestration of carbon. Applied Geochemistry 18, 1065–1080.

Kelemen, P.B., Matter, J., 2008. In situ carbonation of peridotite for CO_2 storage. Proceedings of the National Academy of Science 105, 17295–21730.
Kotra, R.K., Gibson, E.K., Urbancic, M.A., 1982. Release of volatiles from possible Martian analogs. Icarus 51, 593–605.
Lackner, K.S., Butt, D.P., Wendt, C.H., Ziock, H., 1998. Mineral Carbonates as Carbon Dioxide Sinks. Los Alamos National Laboratory, pp. 1–10.
Lide, D.R., 1999. CRC Handbook of Chemistry and Physics, 79th edn.
Liu, Q., Maroto-Valer, M.M., 2010. Investigation of the pH effect of a typical host rock and buffer solution on CO_2 sequestration in synthetic brines. Fuel Processing Technology 91, 1321–1329.
Mandalaparty, P., Deo, M., Moore, J., McPherson, B., 2009. Carbon dioxide Sequestration: Effect of the Presence of Sulfur dioxide on the Mineralogical Reactions and on the Injectivity of $CO_2 + SO_2$ mixtures. University of Utah, Salt Lake City, 53 p.
Maroto-Valer, M.M., 2010a. Developments and Innovation in Carbon dioxide (CO_2) Capture and Storage Technology: Carbon Dioxide (CO_2) Capture, Transport and Industrial Applications. Woodhead Publishing Limited, Cambridge, UK, 538 p.
Maroto-Valer, M.M., 2010b. Developments and Innovation in Carbon dioxide (CO_2) Capture and Storage Technology: Carbon dioxide (CO_2) Storage and Utilisation. Woodhead Publishing Limited, Cambridge, UK, 517 p.
Mazzotti, M., Pini, R., Storti, G., 2009. Enhanced coalbed methane recovery. The Journal of Supercritical Fluids 47, 619–627.
Palandri, J.L., Kharaka, Y.K., 2005. Ferric iron-bearing sediments as a mineral trap for CO_2 sequestration: iron reduction using sulfur-bearing waste gas. Chemical Geology 217, 351–364.
Palandri, J.L., Reed, M.H., 2004. Geochemical models of metasomatism in ultramafic systems: serpentinization, rodingitization, and sea floor carbonate chimney precipitation. Geochimica Et Cosmochimica Acta 68, 1115–1133.
Palandri, J.L., Rosenbauer, R.J., Kharaka, Y.K., 2005. Ferric iron in sediments as a novel CO_2 mineral trap: CO_2–SO_2 reaction with hematite. Applied Geochemistry 20, 2038–2048.
Pruess, K., Xu, T., Apps, J., Garcia, J., 2001. Numerical modeling of aquifer disposal of CO_2. In: SPE/EPS/DOE Exploration and Environmental Conference, San Antonio, TX, pp. 1–14.
Reed, M.H., Spycher, N.F., 2006. Users Guide for CHILLER: A Program for Computing Water-Rock Reactions, Boiling, Mixing and Other Reaction Processes in Aqueous-Mineral-Gas Systems and Minplot Guide, third edition. University of Oregon, Eugene, 67 p.
Reichle, D., Houghton, J., Kane, B., Ekmann, J., et al., 1999. Carbon Sequestration Research and Development. DOE, US.
Rosenbauer, R.J., Koksalan, T., Palandri, J.L., 2005. Experimental investigation of CO_2-brine-rock interactions at elevated temperature and pressure: Implications for CO_2 sequestration in deep-saline aquifers. Fuel Processing Technology 86, 1581–1597.
Rosenbauer, R.J., Thomas, B., 2010. Carbon dioxide (CO_2) sequestration in deep saline aquifers and formations. In: Maroto-Valer, M.M. (Ed.), Developments and Innovation in Carbon dioxide (CO_2) Capture and Storage Technology. Woodhead Publishing Limited, Cambridge, UK, pp. 57–103.
Shock, E.L., Sassani, D.C., Willis, M., Sverjensky, D.A., 1997. Inorganic species in geologic fluids: correlations among standard molal thermodynamic properties of aqueous ions and hydroxide complexes. Geochimica Et Cosmochimica Acta 61, 907–950.
Smith, F.G., Kidd, D.J., 1949. Hematite-goethite relations in neutral and alkaline solutions under pressure. American Mineralogist 34, 403–412.
Spycher, N.F., Reed, M.H., 1988. Fugacity coefficients of H_2, CO_2, CH_4, H_2O and of H_2O–CO_2–CH_4 mixtures – a virial equation treatment for moderate pressures and temperatures applicable to calculations of hydrothermal boiling. Geochimica Et Cosmochimica Acta 52, 739–749.
Stumm, W., Morgan, J.J., 1996. Aquatic Chemistry: Chemical Equilibria and Rates in Natural Waters, third edn. Wiley-Interscience, New York.
Summers, C.A., Dahlin, D.C., Ochs, T.L., 2004. The effect of SO_2 on mineral carbonation in batch tests. In: 29th International Technical Conference on Coal Utilization and Fuel Systems, Coal Technology Association, Gaithersburg, MD, p. 10.
Sun, W., Nesic, S., Woollam, R.C., 2009. The effect of temperature and ionic strength on iron carbonate ($FeCO_3$) solubility limit. Corrosion Science 51, 1273–1276.
Suto, Y., Liu, L., Yamasaki, N., Hashida, T., 2007. Initial behavior of granite in response to injection of CO_2-saturated fluid. Applied Geochemistry 22, 202–218.
Tanger, J.C., Helgeson, H.C., 1988. Calculation of the thermodynamic and transport-properties of aqueous species at high-pressures and temperatures – revised equations of state for the standard partial molal properties of ions and electrolytes. American Journal of Science 288, 19–98.
Van Houten, F.B., 1973. Origin of red beds: a review – 1961–1972. Annual Review of Earth and Planetary Sciences 1, 39–61.
Watts, J.F., Wolstenholme, J., 2003. An Introduction to Surface Analysis by XPS and AES. John Wiley & Sons Ltd., Chichester, UK.
Weast, R.C., 1984. CRC Handbook of Chemistry and Physics, 64th edn. CRC Press Inc., FL, USA.